



HAL
open science

Free-shaped polygonal seismic horizon reconstruction using space transformations

Salma Doghraj, Marc Donias, Sébastien Guillon

► **To cite this version:**

Salma Doghraj, Marc Donias, Sébastien Guillon. Free-shaped polygonal seismic horizon reconstruction using space transformations. *Journal of Applied Geophysics*, 2019, 167, pp.152-159. 10.1016/j.jappgeo.2018.07.021 . hal-02509424

HAL Id: hal-02509424

<https://hal.science/hal-02509424>

Submitted on 25 Oct 2021

HAL is a multi-disciplinary open access archive for the deposit and dissemination of scientific research documents, whether they are published or not. The documents may come from teaching and research institutions in France or abroad, or from public or private research centers.

L'archive ouverte pluridisciplinaire **HAL**, est destinée au dépôt et à la diffusion de documents scientifiques de niveau recherche, publiés ou non, émanant des établissements d'enseignement et de recherche français ou étrangers, des laboratoires publics ou privés.



Distributed under a Creative Commons Attribution - NonCommercial 4.0 International License

FREE-SHAPED POLYGONAL SEISMIC HORIZON RECONSTRUCTION USING SPACE TRANSFORMATIONS

Salma Doghraj¹, Marc Donias¹ and Sébastien Guillon²

¹Univ. Bordeaux, IMS, UMR 5218, F-33400, Talence, France
Bordeaux INP, IMS, UMR 5218, F-33400, Talence, France
CNRS, IMS, UMR 5218, F-33400, Talence, France

²TOTAL, CSTJF, Avenue Larribau, 64000 Pau, France

ABSTRACT

In the context of faulted or occluded regions in seismic images, seismic horizon reconstruction requires the use of fast interactive approaches with respect to any bounding domain and number of passing points. The only algorithms which respect these constraints and provide a result in reasonable time in comparison with the interaction are based on the solution of a partial derivative equation either on juxtaposed quadrangular regions or using a binary mask on the whole data. While the first method requires the use of many passing points and its local nature leads to different results depending on the number and location of constraints, the second is not compatible with fast reconstruction for more than one passing point. In this paper, we propose a global and fast reconstruction method on the polygon defined by constraint points. Direct and inverse Schwarz-Christoffel space transformations lead to global reconstructions in respect to all the constraints. Experiments both on synthetic and real seismic images exhibit better results than the conventional quadrangle and mask methods.

Index Terms— Seismic horizon reconstruction, faulted seismic image, partial derivative equation, space transformation, Schwarz-Christoffel transformation.

1. INTRODUCTION

Seismic images are three-dimensional directional textures representing a stacking of sedimentary layers which appear as a succession of bright and dark surfaces (see figure 1). One key step of interpreting the structure of the subsoil is to reconstruct the frontiers between sedimentary layers, also known as seismic horizon. However, the interpretation process is tedious because of the data dimensionality, seismic faults due to tectonic forces causing horizon disruptions and deaf or chaotic regions. An automatic tool of seismic horizon reconstruction is needed to assist geophysicists during the interpretation stage.

Numerous surface reconstruction methods have been proposed in the literature during the last three decades. Region-

growing methods can be based on the measurement of shape similarity [1, 2] or the integration of the estimated dip [3, 4] starting from an initial point. These methods generally drift because of error cumulation. Methods based on an overall minimization of a nonlinear Partial Derivative Equation (PDE) over the whole solution domain [5, 6, 7, 8, 9] are less noise sensitive.

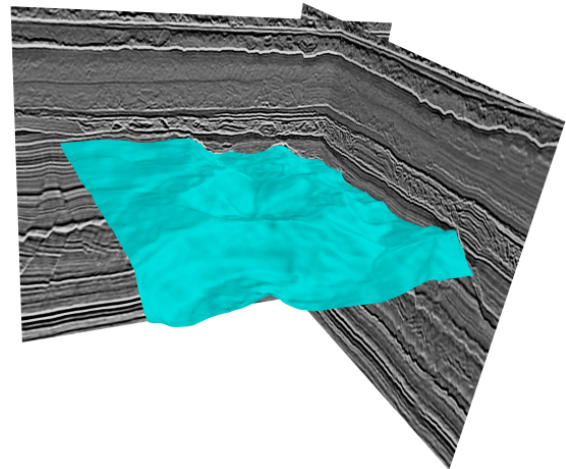


Fig. 1. Seismic horizon (in cyan) reconstructed over seismic image

However, presence of faults, chaotic, noisy or missing regions, requires adding as many passing or domain points as needed. Therefore, only supervised methods allowing a fast reconstruction, which is generally carried out in the Fourier domain and requires a rectangular reconstruction domain, can be used. Moreover, a rectangular domain is not suitable in case of problematic regions. It has to be replaced by a free-shaped domain which occludes or circumvents faulted or problematic regions. Methods of weighted reconstruction can be used on a rectangular domain that surrounds the free-shaped domain by using a weighting function [7] and a particular case using a binary mask [9]. However, in the context of fast reconstruction schemes which are based on the Fourier transform,

weighted reconstruction methods cannot be used with multiple passing points. Moreover, they do not guarantee the convergence of the solution when the normal vector field estimate is highly corrupted by discontinuities and can also introduce numerical instability as well as high computational time. In the general case of supervised methods allowing rapid and interactive consideration of multiple passing points, Zinck *et al.* [10] proposed an approach where the reconstruction domain is defined by the convex polygonal envelope of passing points. Each triangle from Delaunay triangulation of the domain is subdivided into three quadrangles. A partial reconstruction is then performed on each quadrangle by space transformation. This method presents drawbacks due to its local nature. Noise sensitivity depends on the dimensions of each quadrangle and the partial reconstructions derivative continuity is not guaranteed at their boundaries. Moreover, when the configuration changes by adding, changing or deleting a passing point, all the partial reconstructions need to be recomputed.

In [11], we proposed to reconstruct seismic horizons on any simply connected polygonal domain deduced from the free-shaped domain under the constraint of one passing point, using Schwarz-Christoffel (SC) transformations. In this paper, we present the generalization to seismic horizon reconstruction on any simply connected polygonal domain under any number of passing points constraints. Moreover, we discuss SC grid regularization when the SC transformations lead to over-sampled regions. The reconstruction is carried out at once on the whole domain of interest in the Fourier domain using the space transformation and does not extend it to make it convex. In this sense, it is more stable and can be qualified as global.

In the rest of this paper, we first present seismic horizon reconstruction under any kind of bijective differentiable space transformation. Then, we discuss the space transformation between a polygonal domain and rectangular domain before presenting the grid regularization transformation to improve the regularity of the grid corresponding to the SC transformation. In section 3, we compare results of our method to those of the mask and quadrangle methods both on synthetic and real seismic images.

2. SEISMIC HORIZON RECONSTRUCTION IN PRESENCE OF PROBLEMATIC REGIONS

The reconstruction of seismic horizons using the method of [7] is based on the solution of a non linear constrained optimization problem. It relies on the orientation field of the seismic image and refers to a Poisson PDE. The solution of the PDE in the Fourier domain can only be carried out on a hyper-rectangular domain.

However, to avoid faults neighboring or occluded regions, the horizon reconstruction support does not, unless in very specific cases, have a rectangular aspect. It is most likely for the reconstruction domain to have a free polygonal shape.

2.1. Seismic horizon reconstruction under a space transformation

In a seismic image, each seismic horizon can be represented by an explicit hypersurface τ_1 defined by $x_N = \tau_1(\mathbf{x})$ upon the domain Ω_1 where $\mathbf{x} = (x_1, \dots, x_{N-1})$ in a N -dimensional vector space. The hypersurface τ_1 is orthogonal at each point to the orientation field \mathbf{n} [9] (see figure 2). An explicit hypersurface τ_1 verifies a non-linear PDE linking the gradient $\nabla(\tau_1)$ to the vector of slopes \mathbf{p}_1 deduced from the orientation field \mathbf{n} [7]:

$$\forall \mathbf{x}^1 = (x_1^1, \dots, x_{N-1}^1) \in \Omega_1, \nabla \tau_1(\mathbf{x}^1) = \mathbf{p}_1(\mathbf{x}^1, \tau_1(\mathbf{x}^1)). \quad (1)$$

where $\forall i \in [1, N - 1]$,

$$p_{1,i} = -\frac{n_i(\mathbf{x}^1)}{n_N(\mathbf{x}^1)}. \quad (2)$$

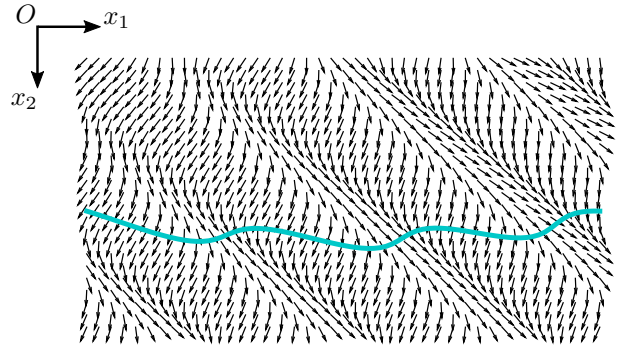


Fig. 2. Explicit hypersurface of a bidimensional orientation field

The seismic horizon is iteratively reconstructed using a non-linear constrained optimization problem:

$$\tau_1 = \underset{g \in C^2}{\operatorname{argmin}} \int_{\Omega_1} \|\nabla g(\mathbf{x}^1) - \mathbf{p}_1(\mathbf{x}^1, g(\mathbf{x}^1))\|^2. \quad (3)$$

Equation 3 refers to a Poisson equation:

$$\Delta(\delta g(\mathbf{x}^1)) = -\operatorname{div}(\nabla g(\mathbf{x}^1) - \mathbf{p}_1(\mathbf{x}^1, g(\mathbf{x}^1))). \quad (4)$$

In general, the minimization of the term in 3 is done using matricial methods. But in the particular case of a rectangular domain, the solution is rapidly deduced using Fourier transforms.

In order to transform an implicit hypersurface into an explicit one or to transform a domain, a space transformation \mathcal{F} from \mathbf{x}^1 into \mathbf{x}^2 can be introduced. Under the conditions of \mathcal{F} being bijective and of class C^1 , a reconstruction is obtained [12] using equation (1) expressed in the transformed space:

$$\forall \mathbf{x}^2 \in \Omega_2, \nabla \tau_2(\mathbf{x}^2) = \mathbf{p}_2(\mathbf{x}^2, \tau_2(\mathbf{x}^2)). \quad (5)$$

Slope vectors are deduced from the components of the orientations $n_j(\mathcal{F}^{-1}(\mathbf{x}^M))$ in the initial space:

$$\forall i \in [1, N-1], p_{2,i} = -\frac{\sum_{j=1}^N \frac{\partial x_j^1}{\partial x_i^2}(\mathbf{x}^2) \cdot n_j(\mathcal{F}^{-1}(\mathbf{x}^2))}{\sum_{j=1}^N \frac{\partial x_j^N}{\partial x_i^2}(\mathbf{x}^2) \cdot n_j(\mathcal{F}^{-1}(\mathbf{x}^2))}. \quad (6)$$

In case of a chain of M bijective space transformations $\mathcal{F} = f_1 \circ \dots \circ f_M$ from \mathbf{x}^1 to \mathbf{x}^{M+1} , the components of the slopes vectors are expressed as:

$$\forall i \in [1, N-1], p_{M+1,i} = -\frac{n_i^{M+1}(\mathbf{x}^{M+1})}{n_N^{M+1}(\mathbf{x}^{M+1})}, \quad (7)$$

where $\mathbf{x}^i = (f_M \circ \dots \circ f_i)^{-1}(\mathbf{x}^{M+1})$. The orientation vectors are expressed as:

$$\mathbf{n}^{M+1} = \mathcal{J}_{M+1}^M(\mathbf{x}^{M+1}) \mathcal{J}_M^{M-1}(\mathbf{x}^M) \dots \mathcal{J}_2^1(\mathbf{x}^2) \mathbf{n}(\mathbf{x}^1), \quad (8)$$

and introduces the terms of the Jacobian \mathcal{J}_{i+1}^i of inverse space transformations f_i^{-1} $i \in [1, M]$:

$$\forall i \in [1, M], \mathcal{J}_{i+1}^i = \begin{bmatrix} \frac{\partial x_1^i}{\partial x_1^{i+1}} & \dots & \frac{\partial x_N^i}{\partial x_1^{i+1}} \\ \vdots & \ddots & \vdots \\ \frac{\partial x_1^i}{\partial x_N^{i+1}} & \dots & \frac{\partial x_N^i}{\partial x_N^{i+1}} \end{bmatrix}. \quad (9)$$

In the following section we present the expression of the bijective transformation between the polygon defined by the constraints and the rectangular domain for fast PDE solution.

2.2. Transformation between a polygon and a rectangle

The Riemann mapping theorem guarantees the existence of a biholomorphic mapping f from any non-empty simply connected subset of \mathbb{C} onto the unit disc D . This implies that f is angle-preserving and is, therefore, a conformal transformation. The SC transformation which was independently discovered by the german mathematicians Christoffel and Schwarz in late 1860s defines an analytic expression of this conformal transformation [13]. Ever since, it has been used in the solution of Laplacian PDE in studies such as Brownian motion [14] and wind flow [15].

The transformation of the polygonal into the rectangular domain can be seen as the compose of two SC transformations which is also a conformal transformation. The first is the inverse SC transformation f_P^{-1} from the polygon P into the unit disc D and the second is the direct SC transformation f_R of D into the rectangle R :

$$\mathcal{F} = f_P^{-1} \circ f_R. \quad (10)$$

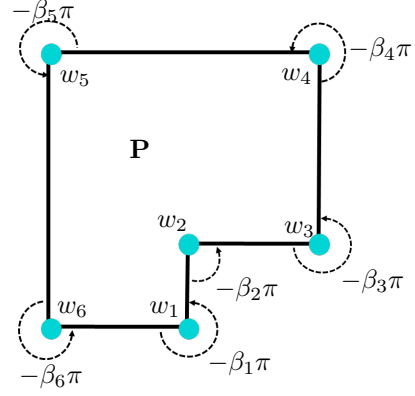


Fig. 3. Polygon P defined by its vertices (in cyan) and exterior angles

Let P be a polygon defined by its vertices w_1, w_2, \dots, w_N (see figure 3). Each vertex w_k has an exterior angle of $-\beta_k \pi$. Note that $\sum_{k=1}^N \beta_k = -2$.

The SC transformation formula defines the conformal transformation of the unit disc D into the polygon P as fol-

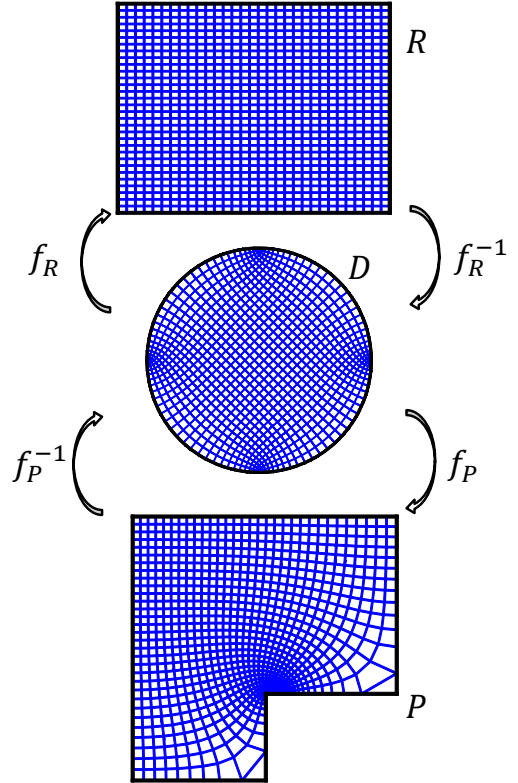


Fig. 4. Transformation of a rectangle R into an L-shaped polygon P using SC transformations

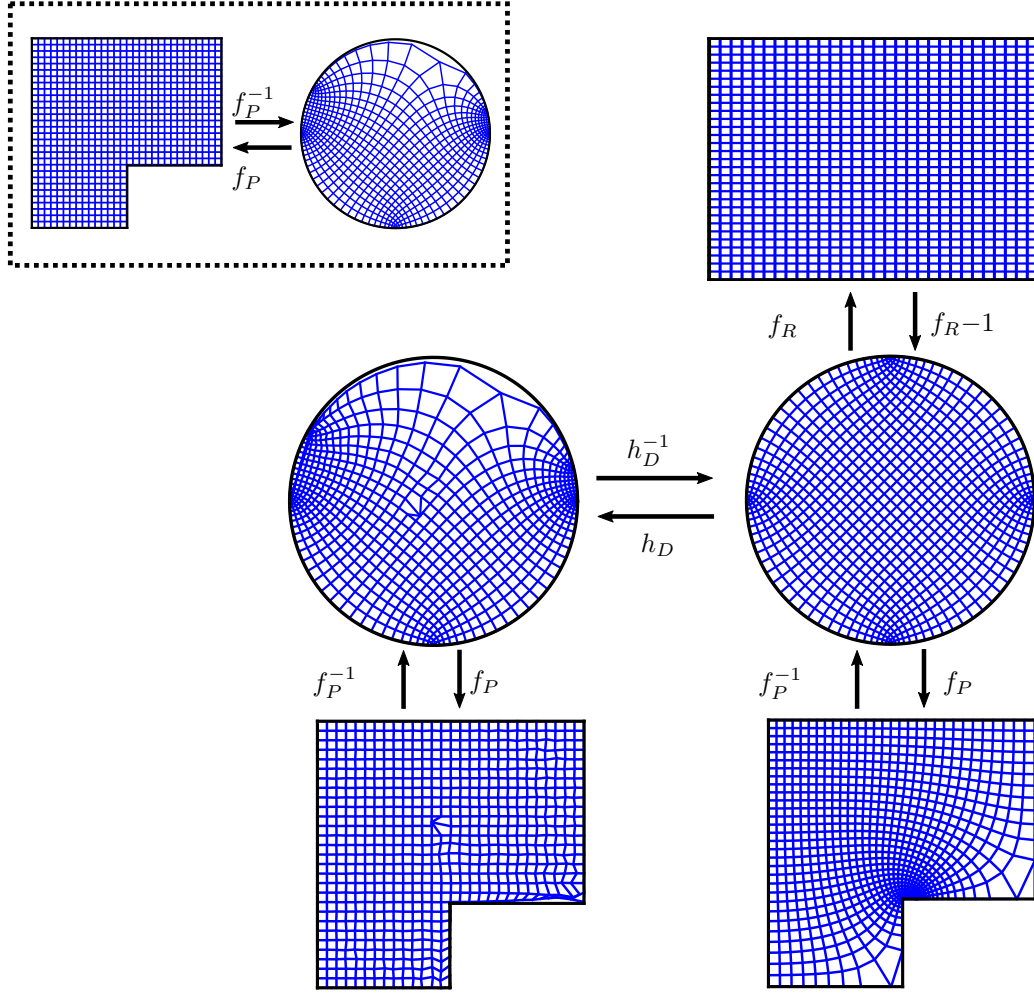


Fig. 5. Transformation of a rectangle into a polygon without regularization and with regularization h_D based on the SC transformation of the polygon (in dotted frame)

lows:

$$\forall z \in D, f_P(z) = a + c \int_0^z \prod_{i=1}^N \left(1 - \frac{s}{z_k}\right)^{\beta_k} ds, \quad (11)$$

where $a, c \in \mathbb{C}$ and $\{z_k\}_{k=1, \dots, N}$ are the pre-images of the vertices of P and are called prevertices. The main task in the definition of the SC transformation is the estimation of the previous $N + 2$ parameters. This is known as the SC parameters problem and is at the heart of the numerical computation of the SC transformation especially as the number of vertices gets higher. However, Trefthen [13] proposed a fast method of numerical solution based on side-length equations after fixing

the values of a and c as $a = f_P(w_1)$ and $c = f_P(w_N)$:

$$\frac{\left| \int_{z_k}^{z_{k+1}} f'_P(z) dz \right|}{\left| \int_{z_1}^{z_2} f'_P(z) dz \right|} = \frac{|w_{k+1} - w_k|}{|w_2 - w_1|}, k = 1, 2, \dots, N - 1 \quad (12)$$

which is solved using the Gauss-Newton method and a Broyden jacobian update. Integration is computed using Gauss-Jacobi method.

The inverse SC transformation corresponds to the computation of $f_P^{-1}(w)$ which is obtained from the differentiation and inversion of $w = f_P(z)$:

$$\frac{dw}{dz} = c \prod_{i=1}^N \left(1 - \frac{s}{z_k}\right)^{\beta_k} \Rightarrow \frac{dz}{dw} = \frac{1}{c} \prod_{i=1}^N \left(1 - \frac{s}{z_k}\right)^{-\beta_k}. \quad (13)$$

This equation is solved numerically using the Newton iterative method starting from a rough approximation \tilde{z} of the

solution obtained from a Runge-Kutta initialization.

Figure 4 shows the SC transformations between an L-shaped polygon P and a rectangle R under the space transformation \mathcal{F} . The SC transformations of the rectangle lead to a highly irregular grid on the polygonal domain. Orientations at some points of the initial grid in the polygon P are not used while others have multiple contributions. This leads to variable reconstruction precision across the domain.

2.3. Grid regularization

An intuitive solution would be to increase the number of sampling points. For instance, if the reconstruction error using a grid of N_P points is ε , then $4 \times N_P$ points should be considered to achieve an $\frac{\varepsilon}{2}$ error. In general, to achieve an $\frac{\varepsilon}{2^n}$, $n \in \mathbb{N}$ error, $2^{2n} \times N_P$ should be considered. This leads to a very high computational complexity compared to the reconstruction accuracy improvement.

Therefore, we introduce an intermediate space transformation h_D between the direct and inverse SC transformation in order to regulate the grid without losing the domain geometry or changing the resolution grid size N_P .

Let us consider the polar coordinates (ρ_{in}, θ_{in}) of the grid corresponding to the transformation f_P^{-1} of the regular grid of P (see figure 5). The objective is to estimate the parameters of a transformation that regularizes the distribution of the disk D in the polar domain without altering the image of the polygon vertices. Therefore $h_D : (\rho_{in}, \theta_{in}) \mapsto (\rho_{out}, \theta_{out})$.

$$\theta_{out} = \theta_{in} + \sum_{k=1}^N u(\beta_k) \mathcal{N}_f(\beta_k, \sigma_{\theta_k}), \quad (14)$$

where $\mathcal{N}_f(\mu, \sigma)$ is a folded normal-distribution of mean μ and standard-deviation σ and the function u is defined by analyzing the angular distribution θ_{in} . Noting $\beta_{N+1} = \beta_1$, the function u can be written:

$$u(\beta_k) = \begin{cases} 1 & \text{if } \theta_{in} \text{ is increasing on } [\beta_k, \beta_{k+1}] \\ -1 & \text{if } \theta_{in} \text{ is decreasing on } [\beta_k, \beta_{k+1}] \\ 0 & \text{else} \end{cases} \quad (15)$$

In the same manner, the radial distribution is changed when the angular distribution is, unless the radius is equal to 1:

$$\rho_{out} = \rho_{in} + \sum_{k=1}^N |u(\beta_k)| \mathcal{N}(\rho_k, \sigma_{\rho_k}), \quad (16)$$

where $\mathcal{N}(\mu, \sigma)$ is a normal-distribution of mean μ and standard-deviation σ , $\rho_k = \frac{1+\rho_{kmin}}{2}$, ρ_{kmin} is the minimal radius corresponding to the angles $\beta_{out} \neq \beta_{in}$ on $[\beta_k, \beta_{k+1}]$ and $\sigma_{\rho_k} = \frac{1-\rho_k}{3}$.

This grid regularization method proves to be efficient, however its implementation can be labourious because of the empirical choice of parameters $u(\beta_k), \sigma_{\theta_k}, \sigma_{\rho_k}$ which are relative to the number of vertices N .

2.4. Computational complexity

Table 1 shows SC transforms computational complexity for a grid of N_P points. The direct transform has roughly a numerical complexity of $O(N_P)$. The inverse transform is first based on the computation of the direct transform and the inversion has a complexity of $O(N_P \times N)$.

| Stage | Method | Complexity |
|-------------------|----------------------------|----------------|
| Parameter problem | Gauss-Jacobi integration | N_P |
| | Broyden Jacobian update | $\sqrt{N_P}$ |
| Integration | Gauss-Jacobi integration | N_P |
| Inversion | Runge-kutta initialization | N_P |
| | Newton iteration | $N_P \times N$ |

Table 1. Computational complexity of the steps of direct and inverse SC transformations

The angular and radial regularization have $O(N)$ complexity. The SC direct and inverse transformations are computed once to estimate the terms $\mathbf{x}^i, i \in [2, M + 1]$. The Jacobians of the direct and inverse SC transformations are computed by differentiation. Both transformations are evaluated 4 times for that matter. The reconstruction has a $N_P \log(N_P)$ computational complexity. The proposed method has, therefore, $N_p(5(N + 1) + \log N_p)$ complexity.

This complexity is to compare to the quadrangle method for which the reconstruction has $\sum_{k=1}^{3(N-2)} N_{Q_k} \log(N_{Q_k})$ where N_{Q_k} is the number of grid points in the k^{th} quadrangle. For each quadrangle the space transformation and corresponding Jacobian need to be computed. They have linear complexity. Overall, both methods have comparable computational execution time in practice.

3. RESULTS

3.1. Results on a synthetic seismic image

First, results are presented on a synthetic $300 \times 300 \times 300$ image with high variations (see figure 6). The theoretical fault appears in red and some theoretical horizons are presented in blue.

The reconstruction using the proposed method has a polygonal domain (see figure 7) taken in order to circumvent the fault. The mask for the method of [9] is defined by setting to 0 the contribution of external points to the polygon in the corresponding rectangular domain.

This results in a shifted horizon using the mask method since the normals are disturbed by the presence of the fault. Even though the reconstruction is less accurate in regions where the SC transformation results in a larger sampling, the

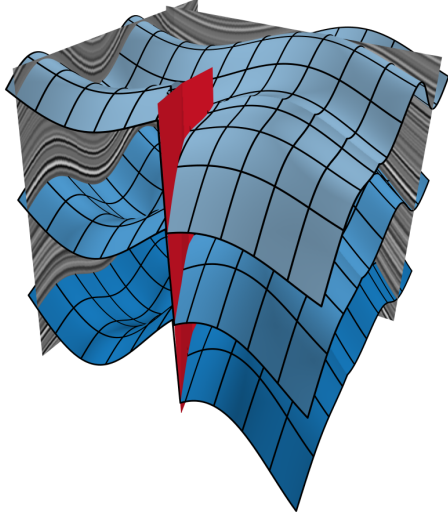


Fig. 6. Faulted synthetic seismic volume, fault model (in red) and some horizons (in blue)

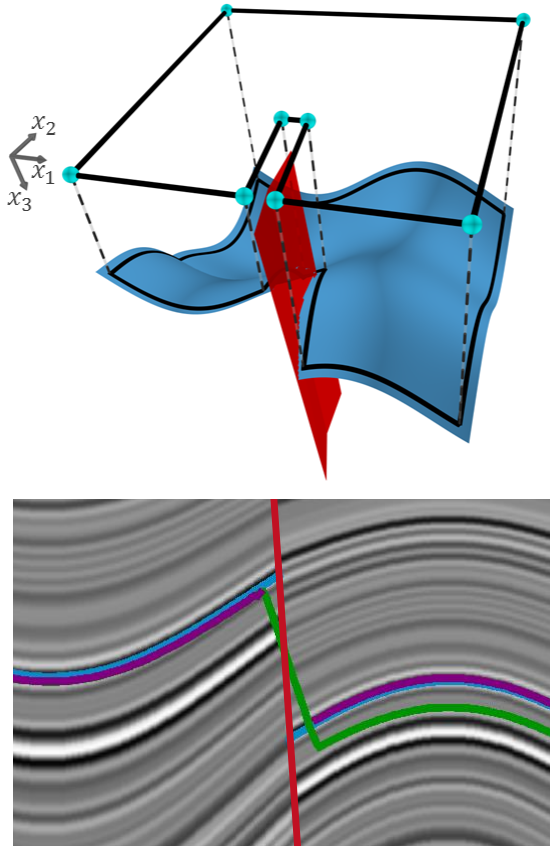


Fig. 7. Top: polygonal reconstruction domain defined by the vertices (in blue) projected on the analytic surface to reconstruct. Bottom: faulted seismic horizon reconstructions - theoretical (in blue), using the mask method (in green) and the proposed method (in indigo) - on the 20^{th} x_2 -section

proposed method leads to better results. The mean quadratic error term compared to the analytic horizons is 0.18 pixels using the proposed method when the binary mask method results in a mean quadratic error of 0.97 pixels.

3.2. Results on real seismic images

In this section, we consider a $329 \times 376 \times 195$ faulted seismic image with regions of occlusion (see figure 8). For the remainder of this paper, each voxel corresponds to a physical dimension of 10 meters in each direction. Since both the faults and the occluded regions are quasi-vertical, we reconstruct the seismic horizon on the domain in figure 8 and one passing point on coordinates (194, 208, 90). We compare the results of our method to those of the mask method with the same passing point and binary mask defined by the polygon of figure 8.

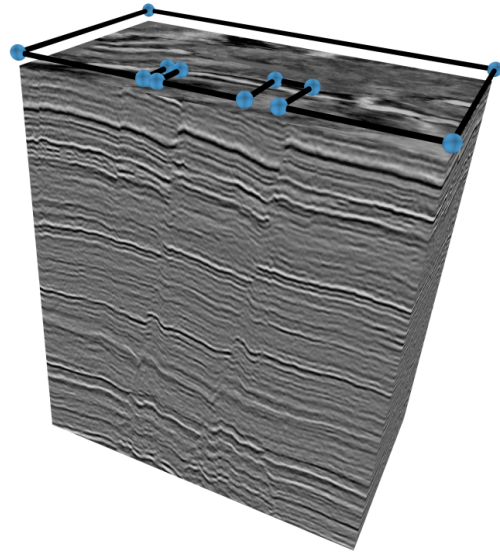


Fig. 8. Faulted seismic image with occluded and faulted regions and polygonal domain

Results of figure 9 show that the reconstructions using the PDE method without and with mask method lead to surfaces that drift away from the observed horizon after the faulted region when our method leads to good results all over the reconstructed region. This is due to the fact that even though the same points are used for the mask and the proposed methods, they do not have the same neighboring. The highest reconstruction differences are located on the sections crossed by faults with a mean absolute difference of 2.43 pixels compared with the mask method and 3.16 pixels without mask.

In the rest of this section, we compare our method to the quadrangle method for a $400 \times 350 \times 400$ real seismic image which contains faults and complex trench structures (figure 10).

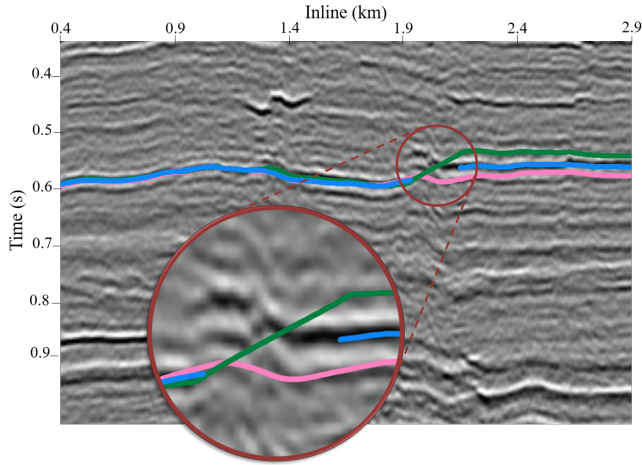


Fig. 9. Faulted seismic horizon reconstructions using the classic PDE method without mask (in pink), with mask (in green) and the proposed method (in blue) on the 172th x_2 -section

The reconstruction domain could be defined automatically by detecting fault position using orientation coherence, gradient magnitude or even trace similarity, as some authors proposed in the literature [16, 17, 18, 19] combined with fault slip estimation as in [20]. In this section, we suppose that the fault location is already known and that the reconstruction domain is defined by passing points of figure 10 which form a non-convex polygon of 9 vertices. The orientation field is estimated using the conventional structure tensor method with standard-deviations of 1 and 2 for the gradient field estimation and autocorrelation matrix computation respectively. Reconstructions are obtained after 40 iterations in the Fourier domain.

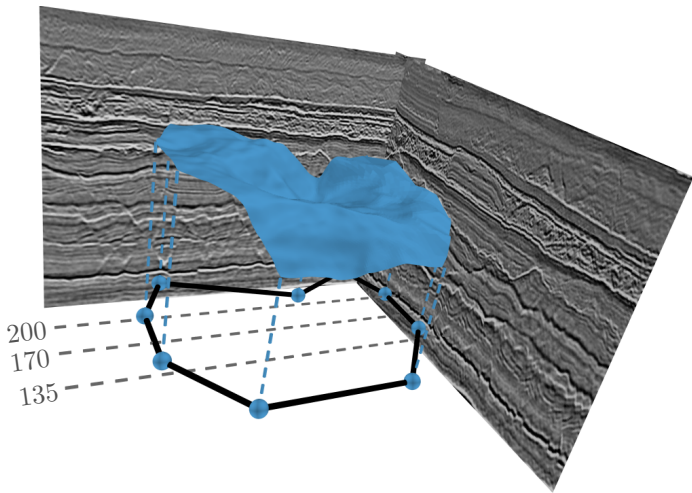


Fig. 10. Seismic image sections and seismic horizon reconstructed on the polygonal domain defined by passing points (in cyan). x_2 -sections of figure 13 (in dotted lines)

For the proposed method, the reconstruction has 410×320 sampling points. The obtained quadrangles using Delaunay triangulation are presented in figure 11. The non-convex domain is transformed into a convex one by adding the region in red which leads to additional partial reconstructions. The sampling grid is imposed by the largest side of the quadrangle which leads to dense but non-homogeneous resolution along partial reconstructions (see figure 12).

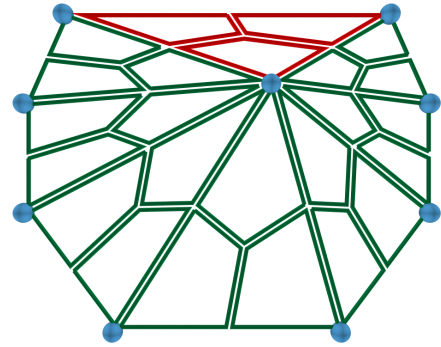


Fig. 11. Quadrangles deduced from Delaunay triangulation of passing points (in blue) - quadrangles inside concave polygon (in green) and outside (in red) -

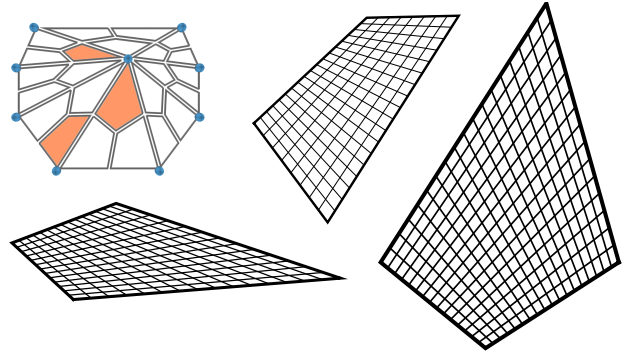


Fig. 12. Sampling independence between the polygon's quadrangles

Figure 13 shows the results of the reconstruction using our quasi-global approach compared with the quadrangle method on different inlines. It appears that the local aspect of the quadrangle method leads to reconstructions that drift away from the observed horizon. SC transformations lead to under-sampled regions (to the left of the polygonal domain). This affects reconstruction accuracy in these regions. Our method with grid regularization leads to better horizon reconstruction and corrects reconstruction errors in under-sampled regions with the SC transformations.

The absolute difference between our method and the quadrangle method highlights up to 11 pixels difference locally and a mean absolute difference of 2.48 pixels on this domain.

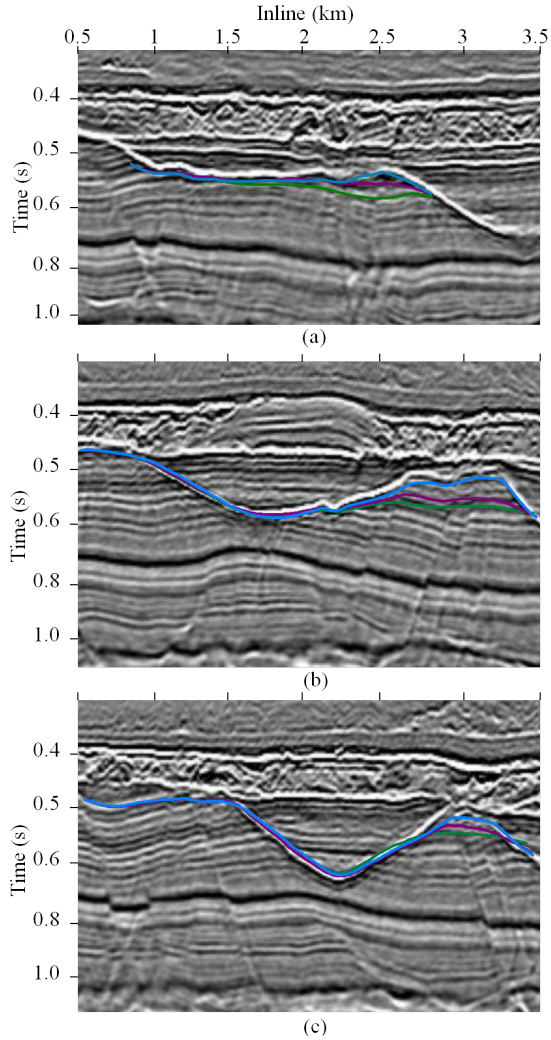


Fig. 13. Reconstructed seismic horizons using the quadrangle method (in green) and our method without (in indigo) and with (in blue) regularization on 135th (a), 170th (b) and 200th (c) x_2 -sections

4. CONCLUSION

We proposed in this paper a fast and global method for seismic horizon reconstruction on any simply connected polygonal domain defined by passing points constraints. Our approach is based on an overall minimization of a partial derivative equation combined with direct and inverse Schwarz-Christoffel transformations beside a bijective grid regularization transformation. Results both on synthetic and real seismic images show better horizon reconstruction when compared with the mask and quadrangle method.

A possible improvement could be carried out by automatic detection and correction of regions where the grid is not regular enough by adopting a regularity criteria and using gradient descent methods.

The simply connected aspect of the domain implies that the fault can be circumvented by a simply connected polygon and that the fault does not bisect the reconstruction domain. If the fault does not intersect any edge of the reconstruction domain, the corresponding polygon would be doubly connected. We address this limitation in [21] using the Schwarz-Christoffel transformation expression in case of a doubly connected polygon. In case the domain is multiply connected, one solution would be to use the expression of the Schwarz-Christoffel transformation for multiply connected domains. Although computational complexity of estimating the parameters of this transformation is large, numerical estimation is likely to be possible in a reasonable amount of time within the relatively near future.

5. ACKNOWLEDGEMENT

The authors would like to thank TOTAL company for funding this research and providing seismic data.

6. REFERENCES

- [1] Hilde G. Borgos, Thorleif Skov, and Trygve Randen, "Automated geometry extraction from 3d seismic data," *73rd Annual International Meeting, SEG, Expanded Abstracts*, pp. 1541–1544, 2003.
- [2] Fabien Pauget, Sébastien Lacaze, and Thomas Valding, "A global approach in seismic interpretation based on cost function minimization," *Society of Exploration Geophysicists*, vol. 28, no. 1, pp. 2592–2596, 2009.
- [3] Nataniello Bienati and Umberto Spagnolini, "Traveltime picking in 3-d data volume," *60th EAGE Meeting, Session : 1-12, Extended Abstracts*, pp. 98–112, 1998.
- [4] Alexander Blinov and Maria Petrou, "Reconstruction of 3-d horizons from 3-d seismic datasets," *IEEE transactions on geoscience and remote sensing*, vol. 43, no. 6, pp. 1421–1431, 2005.
- [5] Michael Kass, Andrew Witkin, and Demetri Terzopoulos, "Snakes: Active contour models," *International journal of computer vision*, vol. 1, no. 4, pp. 321–331, 1988.
- [6] Stanley Osher and James A. Sethian, "Fronts propagating with curvature-dependent speed: algorithms based on hamilton-jacobi formulations," *Journal of computational physics*, vol. 79, no. 1, pp. 12–49, 1988.
- [7] Jesse Lomask and Antoine Guitton, "Flattening with geological constraints," *2006 SEG Annual Meeting. Society of Exploration Geophysicists*, 2006.
- [8] Xinming Wu and Dave Hale, "Horizon volumes with interpreted constraints," *Geophysics*, vol. 80, no. 2, pp. IM21–IM33, 2015.
- [9] Guillaume Zinck, *Reconstruction d'hypersurfaces de champs de normales sous contraintes – Application à l'analyse stratigraphique des images sismiques*, Ph.D. thesis, Univ. Bordeaux, 2012.

- [10] Guillaume Zinck, Marc Donias, Jacques Daniel, Sébastien Guillon, and Olivier Laviolle, “Fast seismic horizon reconstruction based on local dip transformation,” *Journal of Applied Geophysics*, vol. 96, pp. 11–18, 2013.
- [11] Salma Doghrajji and Marc Donias, “Seismic horizon reconstruction on polygonal domains using the schwarz-christoffel transformation,” *International Conference on Image and Signal Processing*, pp. 4057–4061, 2016.
- [12] Guillaume Zinck, Marc Donias, and Olivier Laviolle, “N-dimensional surface reconstruction from a noisy normal vector field,” *20th European Signal Processing Conference (Eusipco-2012)*, pp. 395–399, 2012.
- [13] Tobin A. Driscoll and Lloyd N. Trefethen, *Schwarz-Christoffel Mapping*, Cambridge Monographs on applied and Computational Mathematics, 2002.
- [14] Lloyd N. Trefethen and Ruth J. Williams, “Conformal mapping solution of laplace's equation on a polygon with oblique derivative boundary conditions,” *Journal of Computational and Applied Mathematics*, vol. 14, no. 1, pp. 227–249, 1986.
- [15] Aaron Waters, François Blanchette, and Arnorld D. Kim, “Modeling huddling penguins,” *Applied Mathematics, University of California Merced*, vol. 7, no. 11, 2012.
- [16] Kurt J Marfurt, R Lynn Kirlin, Steven L Farmer, and Michael S Bahorich, “3-d seismic attributes using a semblance-based coherency algorithm,” *Geophysics*, vol. 63, no. 4, pp. 1150–1165, 1998.
- [17] Trygve Randen, Stein Inge Pedersen, Lars Sønneland, et al., “Automatic extraction of fault surfaces from three-dimensional seismic data,” in *2001 SEG Annual Meeting*. Society of Exploration Geophysicists, 2001.
- [18] David Gibson, Michael Spann, Jonathan Turner, and Timothy Wright, “Fault surface detection in 3-d seismic data,” *IEEE Transactions on Geoscience and Remote Sensing*, vol. 43, no. 9, pp. 2094–2102, 2005.
- [19] Dave Hale, “Methods to compute fault images, extract fault surfaces, and estimate fault throws from 3d seismic images,” *Geophysics*, vol. 78, no. 2, pp. O33–O43, 2013.
- [20] Xinming Wu and Dave Hale, “3d seismic image processing for faults,” *Geophysics*, vol. 81, no. 2, pp. IM1–IM11, 2016.
- [21] Salma Doghrajji, *Caractérisation de la géométrie locale et globale de textures directionnelles par reconstruction d'hypersurfaces et transformations d'espace - Application à l'analyse stratigraphique des images sismiques*, Ph.D. thesis, Univ. Bordeaux, 2017.